

UC Santa Cruz

UC Santa Cruz Previously Published Works

Title

Disruption and reaccretion of midsized moons during an outer solar system Late Heavy Bombardment

Permalink

<https://escholarship.org/uc/item/464367jj>

Journal

Geophysical Research Letters, 42(2)

ISSN

00948276

Authors

Movshovitz, N.
Nimmo, F.
Korycansky, D. G
et al.

Publication Date

2015-01-28

DOI

10.1002/2014GL062133

Peer reviewed

1 Disruption and re-accretion of mid-sized moons
2 during an outer Solar System Late Heavy
3 Bombardment

N. Movshovitz,¹ F. Nimmo,¹ D. G. Korycansky,¹ E. Asphaug,² and J. M.
Owen³

Corresponding author: N. Movshovitz, Department of Earth and Planetary Sciences, University of California Santa Cruz, Santa Cruz, CA 95064, USA. (nmovshov@ucsc.edu)

¹Department of Earth and Planetary
Sciences, University of California Santa
Cruz, Santa Cruz, CA 95064, USA.

²School of Earth and Space Exploration,
Arizona State University, Tempe, AZ 85287,
USA.

³Lawrence Livermore National
Laboratory, Livermore, CA 94550, USA.

4 We investigate the problem of satellite survival during a hypothetical late
5 heavy bombardment in the outer solar system, as predicted by the Nice Model
6 (Tsiganis, Gomes, Morbidelli, & Levison 2005, Nature 435). Using a Monte-
7 Carlo approach we calculate, for satellites of Jupiter, Saturn, and Uranus,
8 the probability of experiencing a catastrophic collision during **the** LHB. We
9 find that Mimas, Enceladus, Tethys, and Miranda experience at least one
10 catastrophic impact in every simulation. Because re-accretion is expected to
11 be rapid, these bodies will have emerged as scrambled mixtures of rock and
12 ice. Tidal heating may have subsequently modified the latter three, but in
13 the nominal LHB model Mimas should be a largely undifferentiated, homo-
14 geneous body. A differentiated Mimas would imply either that this body formed
15 late, or that the Nice model requires significant modification.

1. Introduction

16 The lunar Late Heavy Bombardment (LHB; the apparent clustering of lunar basin ages
17 around 3.9 Ga) can be explained by a model [*Tsiganis et al.*, 2005; *Gomes et al.*, 2005]
18 that invokes a period of dynamical instability occurring long after planet formation. In
19 this model, often called the Nice Model, the giant planets are formed in circular orbits,
20 all inside of 20 AU, while an exterior disk of unaccreted planetesimals remains beyond
21 30 AU. Scattering of planetesimals due to chance encounters results in slow migration
22 of the giant planets until Jupiter and Saturn reach a 1:2 mean motion resonance. The
23 resulting dynamical instability destabilizes both the asteroid main belt and the exterior
24 planetesimal disk. A careful choice of initial conditions can delay the onset of instability
25 to about 700 My after planet formation, delivering enough planetesimal mass to the
26 Earth-Moon system at 3.9 Ga to cause the lunar LHB [*Gomes et al.*, 2005].

27 The above scenario also predicts an LHB-like period in the outer Solar System. In fact,
28 the higher collision probabilities and impact energies due to gravitational focusing by the
29 giant planets suggest that the inner satellites of Jupiter, Saturn, and Uranus would have
30 experienced a bombardment much more severe than the one supposedly responsible for the
31 lunar basins. The concern is that this outer Solar System LHB should have resulted not
32 just in cratering, but in significant, even catastrophic modification of the smaller satellites
33 [e.g. *Barr and Canup*, 2010; *Nimmo and Korycansky*, 2012]. The general vulnerability
34 of the smaller satellites to catastrophic disruption and re-accretion has been noted by
35 previous authors [e.g. *Smith et al.*, 1982, 1986; *Zahnle et al.*, 2003], and the probability
36 of satellite survival in the context of the proposed 3.9 Ga LHB was also calculated in

37 [*Charnoz et al.*, 2009]. Our contribution is to examine in detail the expected level of
38 destruction experienced by each satellites.

39 In a previous study *Nimmo and Korycansky* [2012] have shown, using estimates of
40 impactor populations [*Charnoz et al.*, 2009], collision probabilities [*Zahnle et al.*, 2003],
41 and a scaling law for impact-induced vapor production [*Kraus et al.*, 2011], that several
42 satellites (Mimas, Enceladus, Miranda) should have lost most of their ice content during
43 the LHB, unless the total mass delivered to the outer Solar System was a factor of 10
44 smaller than predicted by the original Nice Model [*Barr and Canup*, 2010; *Dones and*
45 *Levison*, 2013].

46 In this work we look again at the problem of satellite survival, this time focusing on
47 disruption rather than vaporization. We calculate the probability of a satellite experi-
48 encing one or more impacts energetic enough to disperse more than 50% of the target's
49 mass (not necessarily vaporized). We find that disruption is much more dangerous than
50 vaporization, particularly for the inner satellites of Saturn. In fact, it seems very unlikely
51 that these satellites could have survived the nominal LHB unmodified in their present
52 orbits.

2. Method

53 For each satellite of interest we ask: What is the probability of it suffering at least one
54 *catastrophic* collision, defined as a collision that disperses at least half the original target
55 mass, during a hypothetical LHB? To answer this question we need to know the total mass
56 of impactors delivered to the target satellite, the statistics of the impactor population (in
57 particular, the size and velocity distribution of impacting bodies), and the effects of a

58 given impact. We consider each of these elements in turn in the following sections, and
 59 then describe how they are used in a Monte-Carlo simulation of an outer Solar System
 60 LHB.

2.1. Total mass of impactors delivered to each target

61 The Nice model explanation for the lunar LHB requires a rather massive planetesimal
 62 disk external to the orbits of the giant planets. *Gomes et al.* [2005] suggest 35 earth masses
 63 (M_E) in the initial disk. From the output of these simulations, several authors estimate
 64 the mass **expected to strike Saturn** between 0.06 and 0.37 M_E [*Charnoz et al.*, 2009;
 65 *Barr and Canup*, 2010; *Dones and Levison*, 2013]. **Later studies have suggested ways**
 66 **of reducing somewhat the predicted disk mass** [e.g. *Nesvorný*, 2011; *Nesvorný*
 67 *et al.*, 2013]. In this work we treat the total delivered mass as a free parameter, spanning
 68 the range suggested by previous studies **and down to less than one percent of the**
 69 **canonical value.**

70 The mass delivered to each satellite of interest is calculated based on the relative impact
 71 probabilities given by *Zahnle et al.* [2003, their table 1]. *Zahnle et al.* [2003] report
 72 impact probabilities relative to Jupiter, P_{EC}^{sat} . We denote by M_{LHB} the total mass delivered
 73 to Jupiter, and thus $M_{LHB}^{sat} = P_{EC}^{sat} M_{LHB}$. A satellite's relative probability of being hit
 74 scales with the square of its radius and inversely with its orbital distance (assuming an
 75 approximately circular orbit **and strong gravitational focusing by the primary**).

2.2. Mass dispersed by an impact

76 An impact is characterized by the target's mass M and radius R , the impactor's mass
 77 m_i and radius r_i , and the impact velocity v_i (in the target's rest frame) and angle θ . We

78 are interested in the gravity regime where material strength may be ignored. For a given
 79 target, and for impacts in the near-catastrophic regime, it is customary to make the as-
 80 sumption that the outcome is determined by the specific impact energy $Q = (m_i v_i^2)/(2M)$.
 81 More precisely, numerical simulations [*Benz and Asphaug, 1999; Leinhardt and Stewart,*
 82 *2012*] show that, for a given target, the fraction of target mass that remains bound in the
 83 largest post-collision fragment is a linear function of Q :

$$84 \quad \frac{M_{\text{lr}}}{M} = \max\left(0, 1 - 0.5 \frac{Q}{Q_D^*}\right). \quad (1)$$

85 The parameter Q_D^* is the specific energy required to disperse half the target mass, and is
 86 a function of the target radius.

87 In this work we are interested in targets in the 100 to 1000 km range. To extend previous
 88 scaling laws for $Q_D^*(R)$ to this range we carried out a series of hydro-code simulations
 89 between ice bodies in the gravity regime using the parallel, SPH-based code SPHERAL
 90 [*Owen et al., 1998; Owen, 2010, 2014*]. We simulated impacts into targets with $R =$
 91 500 km and $R = 1000$ km. Target and impactor materials were modeled with a Tillotson
 92 equation-of-state using parameters suitable for H₂O ice [*Melosh, 1989*]. For each target
 93 we ran impacts with several specific energies, and for each value of specific energy we
 94 used **two impactors** ($r_i = 250$ km and $r_i = 200$ km) **with different velocities, in**
 95 **order to verify velocity-independent scaling**. Fitting a line to the remaining bound
 96 mass fraction vs. the specific impact energy, we thus determine $Q_D^*(R = 500 \text{ km})$ and
 97 $Q_D^*(R = 1000 \text{ km})$. Figure 1 shows these values next to values obtained previously for
 98 smaller targets by *Benz and Asphaug* [1999, their fig. 4], demonstrating a very good

99 agreement between the different codes. (For more detail about the SPH simulations see
 100 the Supporting Information on line.)

101 We find that, for ice targets in the gravity regime, Q_D^* is well approximated by

$$102 \quad Q_D^* \approx 0.05 \text{ J/kg} \times \left(\frac{R}{1 \text{ m}} \right)^{1.188}. \quad (2)$$

103 The above scaling law is valid for head-on impacts. Oblique impacts can be handled
 104 by considering only the fraction of impactor volume that intersects the target [*Asphaug,*
 105 2010; *Leinhardt and Stewart, 2012*].

106 Consider, for example, Mimas, the innermost satellite of Saturn. It has a radius of
 107 ~ 200 km and a mass of $\sim 3.8 \times 10^{19}$ kg. By eq. (2), $Q_D^* \approx 10^5$ J/kg. **In order**
 108 **of magnitude**, the impact velocity of a heliocentric impactor is the satellite's orbital
 109 velocity, $v_{\text{orb}} \approx 14$ km/s. A single 20 km ice impactor at this velocity carries enough
 110 energy to disperse half the satellite's mass. In the nominal Nice model Mimas is expected
 111 to encounter a total impactor mass equivalent to hundreds of such bodies.

112 In the high-energy but relatively low-velocity impacts simulated here, the ejected mass
 113 is not vaporized. This is not surprising, since significant shock- induced melting and
 114 vaporization of ice requires impact velocities higher than ~ 8 km/s [*Kraus et al., 2011*].
 115 In our numerical simulations it was necessary to use lower (but still supersonic) impact
 116 velocities so that a higher impactor-to-target size ratio can be used – a requirement of
 117 numerical resolution. In reality some vapor production is bound to occur, but most of the
 118 mass ejected by the impact will be in the form of large, solid fragments. Unlike vaporized
 119 material, these fragments are expected to subsequently re-accrete in relatively short time
 120 (see below).

2.3. Impactor size and velocity distribution

121 The simple calculation shown above neglects some important details that may miti-
122 gate the destructive potential of a hypothetical LHB. First, eq. (1) assumes a gravity-
123 dominated impact. If much of the mass delivered by the LHB came in the form of very
124 small (< 1 km) impactors, we may expect heavy cratering but no significant mass loss
125 from impacts. Second, eq. (1) assumes a head-on impact. If much of the delivered mass
126 came in the form of one or two large (comparable to target size) impactors, the angle of
127 impact would play an important role. A chance glancing impact could spend much of
128 the mass budget to minimal effect. We therefore need to consider the statistics of the
129 impactor population.

130 Third, and most important, eq. (1) predicts the mass of material initially escaping the
131 gravity of the target body, but this material is not necessarily gone for good. Heliocentric
132 impactors hit a satellite at roughly the orbital velocity, $v_{\text{imp}} \approx \sqrt{3}v_{\text{orb}}$. Material is ejected
133 at a range of velocities up to about v_{imp} , while the escape velocity from the primary at the
134 orbital distance of the satellite is $v_{\text{esc}}^P = \sqrt{2}v_{\text{orb}}$. Thus much of the material that initially
135 escapes the target goes into a similar orbit about the primary, and will eventually re-
136 accrete. The timescale for re-accretion depends on the initial spread in semi-major axis
137 given to the ejected material, which in turn depends on the velocity distribution of ejected
138 material [e.g. *Gladman and Coffey*, 2009]. But even a conservative estimate puts the re-
139 accretion time scale at no more than some thousands of orbits. This is much shorter than
140 the likely interval between impacts. As a result, although some mass loss may well occur,

141 the main effect of multiple catastrophic impacts followed by prompt re-accretion will be
 142 to disrupt any pre-existing structure. We discuss this possibility further in section 4.

143 **2.3.1. Impactor size distribution**

144 The Nice model’s trans-neptunian planetesimal disk is thought to be the progenitor of
 145 the present-day Kuiper Belt. So the currently observed size distribution in the Kuiper Belt
 146 can serve as a **good starting point for a derived** size distribution of LHB impactors.
 147 Here we adopt the size distribution suggested by *Charnoz et al.* [2009], a distribution scaled
 148 to match the cratering record on Iapetus **and designed to estimate the distribution**
 149 **in the primordial disk.** The cumulative fraction N of planetesimals with radius greater
 150 than r is assumed to be a power law with two break points:

$$151 \quad N(r) = \begin{cases} 1, & r < r_{\min}, \\ r_{\min}^{1.5} r^{-1.5}, & r_{\min} < r < 7.5, \\ 7.5 r_{\min}^{1.5} r^{-2.5}, & 7.5 < r < 100, \\ 750 r_{\min}^{1.5} r^{-3.5}, & 100 < r. \end{cases} \quad (3)$$

152 where r is measured in km and r_{\min} is an arbitrarily chosen smallest impactor. For a given
 153 total mass in the population, the choice of r_{\min} determines the total number of impactors.

154 With this size distribution, less than 0.2% of the mass is found in bodies smaller than
 155 1 km in radius, justifying our use of energy scaling in eq. (1). However, more than 65% of
 156 the mass is found in bodies larger than 100 km, and so we must account for the collision
 157 angle.

158 The implementation of this size distribution is described in full detail in the supporting
 159 information on line.

160 **2.3.2. Impact velocity distribution**

161 The probability distribution of impact velocities is described in *Zahnle et al.* [1998] for
162 hyperbolic impactors with isotropic inclinations, and making some assumptions about the
163 planetesimals' velocities at infinity.

164 The collision angle θ can strongly influence the outcome of a collision. If we assume the
165 canonical $\sin 2\theta$ distribution [*Shoemaker and Wolfe*, 1982], the median collision angle is
166 45 degrees. In oblique impacts between bodies of comparable size, a significant fraction
167 of the impactor volume is sheared off and leaves the scene largely intact. As a result, a
168 significant fraction of the impact kinetic energy is not coupled to the target, and should
169 not be included in Q when calculating the mass ejected by the impact. We deal with this
170 by following the same procedure as in *Leinhardt and Stewart* [2012], considering only the
171 fraction of the impactor mass in the volume intersected by the target at impact.

172 Consider again the case of Mimas, but now assume a 100 km radius impactor. This
173 impactor contains about half the mass the Nice model predicts was delivered to Mimas
174 during an LHB. A head-on impact is easily enough to destroy Mimas many times over.
175 But at an impact angle of 60 degrees only 10% of the impactor volume intersects the
176 target. This effect adds a strong stochastic element to the outcome of an LHB period
177 that we must consider.

2.4. A Monte-Carlo model

178 For each target of interest, we simulate a series of random LHB events and look at the
179 outcome.

180 An LHB event is defined by the total mass delivered to the target, M_{LHB} . This is our
181 main control parameter. We draw a random size, velocity, and angle, from the distribu-

182 tions discussed above. We calculate Q , the effective specific energy of the impact inter-
 183 secting the target, and Q_D^* for the target. If $Q > Q_D^*$ we increment a catastrophic impact
 184 counter. We also keep track of super-catastrophic ($Q > 2Q_D^*$) and ultra-catastrophic
 185 ($Q > 3Q_D^*$) impacts, **to better quantify how much disruption takes place**. The
 186 procedure is repeated until the total mass delivered by impacts exceeds M_{LHB} . The last
 187 impactor may be reduced ad-hoc to avoid overshooting the mass limit.

188 Note that we make the conservative assumption that any ejected mass is quickly re-
 189 accreted. The target's mass and radius thus remain constant throughout the simulation.
 190 This approach is conservative since if the target were allowed to lose mass between impacts
 191 we would have to adjust its Q_D^* according to eq. (2), making it progressively easier to
 192 disrupt.

193 We begin by setting $M_{\text{LHB}}^{\text{sat}}$ for each target scaled to match $M_{\text{LHB}}^{\text{Callisto}} = 3 \times 10^{20}$ kg as
 194 suggested by *Barr and Canup* [2010]. Then we scale down the delivered mass until all
 195 saturnian satellites survive their respective LHBs. For each value of M_{LHB} we ran 200
 196 simulations. The resulting statistics are described below.

3. Results

197 Figure 2 shows the fraction of Monte-Carlo runs that included at least one collision
 198 with energy greater than one, two, or three times Q_D^* , for 11 outer solar system satellites.
 199 Mimas, Enceladus, Tethys, and Miranda experienced a catastrophic impact in every sim-
 200 ulation. In most runs, Mimas, Enceladus, and Tethys experienced *multiple* catastrophic
 201 impacts, including impacts with energy several times that required to completely disrupt
 202 the target. These satellites would be heavily modified by an LHB no matter what as-

203 sumptions we make about the impactor population or re-accretion efficiency. By contrast,
204 the larger satellites (Europa, Ganymede, Callisto and Titan) are not expected to undergo
205 disruption; nor are very distant objects such as Iapetus.

206 **Sentence deleted here.** Figure 3 shows how the probability of catastrophic disruption
207 drops when the total mass delivered in the simulation is reduced. A reduction by a factor
208 of 3 is not enough to save Mimas or Enceladus, nor, probably, Tethys or Dione. Figure 3
209 shows that the mass delivered by a hypothetical LHB must be at least 30 times less than
210 the value predicted by the Nice model to give Enceladus a decent chance of survival, and
211 100 times less to give Mimas any chance at all.

212 **The expected number of destructive events and the overall destruction prob-**
213 **abilities calculated in our Monte-Carlo simulations are much higher than those**
214 **previously reported by *Charnoz et al.* [2009, their Table 3]. The discrepancy**
215 **is mainly due to the different values we calculate for the number of impactors**
216 **larger than a given size expected to hit each satellite. For example, *Charnoz***
217 ***et al.* [2009, their fig. 8] calculate that a 200 km satellite at 100,000 km is**
218 **expected to see about one impact with a 20 km radius comet during the LHB,**
219 **while a similar body in Mimas orbit is expected to see about 0.57 such comets.**
220 **In contrast our Monte-Carlo runs, which are scaled from the 3×10^{20} kg striking**
221 **Callisto, typically result in 30 – 50 such bodies striking Mimas.**

222 **The discrepancy suggests that, for a given primordial disk mass, the total**
223 **mass that we expect to hit all outer planets and their satellites during the**
224 **LHB is larger than the value calculated by *Charnoz et al.* [2009]. With a**

225 primordial disk of 20 Earth masses, the 0.17% probability of impact on Saturn
 226 that Charnoz et al. calculate, translates to about 2×10^{23} kg striking Saturn,
 227 and the relative collision probabilities calculated by Zahnle et al. result in
 228 2.9×10^{19} kg striking Callisto, almost exactly an order of magnitude less than the
 229 value suggested by *Barr and Canup* [2010] based on the original Nice Model.
 230 There may also be other factors contributing to the apparent discrepancy.

3.1. Caveats

231 The results given above were obtained using the specific scaling law for Q_D^* , eq. (2).
 232 This scaling law was derived with hydrocode simulations of impacts, where the equation-
 233 of-state (EOS) plays an important role. We chose to use the Tillotson EOS [*Melosh*, 1989]
 234 because it was the easiest to implement in our code, not because it is the best available
 235 EOS for ice in the pressure and temperature regime of interest [*Senft and Stewart*, 2008].
 236 Our simulations were also focused on ice targets: the parameters given to the Tillotson
 237 EOS were those appropriate for ice [*Melosh*, 1989]. Real targets are likely a mix of ice
 238 and silicates, but an appropriate EOS for an unknown mixture of $\text{H}_2\text{O}/\text{SiO}_2$ is difficult
 239 to construct.

240 To verify the robustness of our results in light of the above caveats, we ran several
 241 Monte-Carlo simulations using a different scaling law. From values given by *Benz and*
 242 *Asphaug* [1999, their Fig. 3] for basalt targets, we fit

$$243 \quad Q_D^* \approx 1.48 \text{ J/kg} \times \left(\frac{R}{1 \text{ m}} \right)^{0.9893}. \quad (4)$$

244 For the targets we are interested in, eq. (4) yields values that are about an order of
 245 magnitude greater than eq. (2). Given the mixed composition of most satellites, we may

246 assume that the two end members, eq. (2) for pure ice and eq. (4) for pure basalt, bracket
247 the real Q_D^* value for any target.

248 Running our simulated LHBs with this upper limit Q_D^* , we find that the probability of
249 many satellites' experiencing a catastrophic impact remains high. In particular, as shown
250 in figure 4, Mimas, Enceladus, Tethys, and Miranda still experience a catastrophic impact
251 in almost every run.

252 Different scaling laws for gravity regime impacts also exist. *Leinhardt and*
253 *Stewart* [2012, hereafter LS12] suggest a velocity-dependent scaling law that
254 increases the disruption threshold for high velocity impacts. The LS12 scaling,
255 however, was based on simulated collisions with targets up to 100 km in radius,
256 and does not agree with our SPH simulations of impacts into larger targets.
257 Nevertheless, we ran our Monte-Carlo simulation using the LS12 scaling as
258 well. As expected, the total number of catastrophic collisions experienced by
259 each target was reduced. But the probability of experiencing at least one such
260 collision remained almost as high as in our baseline case, so our conclusions
261 given in the following section hold with either scaling law. A direct comparison
262 is shown in the Supporting Information on line.

4. Implications

263 Figures 2 and 3 suggest that the inner Saturnian and Uranian satellites were disrupted
264 (and then re-accreted) several times during the putative LHB. Here we enumerate several
265 consequences of this scenario.

266 1. The impact history recorded by these satellites prior to the LHB was erased. This
267 conclusion is not in conflict with existing constraints on surface ages based on cratering
268 rate calculations [*Zahnle et al.*, 2003]. In striking contrast, Iapetus – which is not predicted
269 to undergo disruption – has an anomalously large number of impact basins [*Dones et al.*,
270 2009], perhaps reflecting a contribution from the pre-LHB bombardment not recorded in
271 the inner saturnian satellites. The ancient surface ages inferred for Callisto, Umbriel, and
272 Oberon are also consistent with our results, since these bodies are not expected to have
273 undergone disruption. Pluto and Charon may likewise have old surface ages, their distant
274 orbit, large size, and low gravitational potential making them immune to any LHB.

275 2. Catastrophic disruption and prompt re-accretion is likely to lead to a “scrambled”
276 body in which ice and rock are randomly distributed, and to initially high levels of porosity.
277 For mid-sized satellites, neither the energy of re-accretion nor long-lived radioactive decay
278 are sufficient to cause melting and subsequent differentiation [*Monteux et al.*, 2014; *Nagel*
279 *et al.*, 2004]. Later differentiation could have occurred due to tidal heating (e.g. Enceladus
280 [*Meyer and Wisdom*, 2007], Tethys [*Chen and Nimmo*, 2008], perhaps Miranda [*Dermott*
281 *et al.*, 1988]), while later impacts would have added ice-rich material to the surface.
282 Nonetheless, the LHB implies that the interiors of Mimas and (perhaps) Miranda are
283 largely undifferentiated. This prediction is potentially testable, because shape or gravity
284 measurements can under certain circumstances be used to derive a body’s moment of
285 inertia [*Dermott and Thomas*, 1988]. The shape of Mimas is non-hydrostatic [*Thomas*,
286 2010; *Tajeddine et al.*, 2014], which indicates a relatively cold, stiff body, but does not

287 permit the moment of inertia to be inferred. The shape of Miranda is too uncertain to
288 provide useful information [*Thomas, 1988*].

289 Deep initial porosity will be removed by compression over time. However, even on tidally-
290 heated bodies like Enceladus, there will be a cold, near-surface layer, tens of km thick,
291 in which porosity can survive [e.g. *Besserer et al., 2013*]. Inactive bodies such as Mimas
292 could potentially have a thicker porous layer, thereby reducing their bulk density.

293 3. Although our calculations assume complete re-accretion in order to be conservative,
294 collisions are stochastic and some will surely result in mass loss. In particular, for target
295 bodies that are differentiated, the catastrophic collisions which occurred during the LHB
296 are likely to have affected the ice-to-rock ratio. For instance, the apparently ice-rich nature
297 of Tethys can readily be explained if Tethys is a spall fragment produced during a giant
298 impact on a differentiated body [*Asphaug and Reufer, 2013; Sekine and Genda, 2012*].
299 The satellites that we see today may in some cases be fragments of their former selves.

300 4. We have implicitly assumed that the satellites formed at the same time as the rest
301 of the Solar System i.e. prior to the LHB. One way of avoiding disruption is to posit that
302 the inner satellites formed during or after the LHB. *Charnoz et al. [2011]* and *Crida and*
303 *Charnoz [2012]* suggest that the mid-sized moons of Saturn could have been formed by
304 accretion from a massive, ice-rich ring [*Canup, 2010*] containing large silicate fragments.
305 This scenario is consistent with a late (post-LHB) formation of the inner saturnian satel-
306 lites and predicts a differentiated Mimas. Indeed, post-LHB satellite formation is a natural
307 outcome if the ring progenitor itself were delivered (or disrupted) by the LHB.

5. Conclusions

308 The canonical Nice model scenario for the LHB [*Gomes et al.*, 2005] will have caused
309 multiple catastrophic disruption and prompt re-accretion of many outer solar system
310 satellites, particularly Mimas, Enceladus, Tethys, and Miranda. None of these bodies
311 (unlike, say, Iapetus or Callisto) will have recorded any events on their surface prior to
312 3.9 Ga. The interior structures of Enceladus, Tethys, and Miranda may have been affected
313 by subsequent tidal heating events, but the internal structure of Mimas is predicted to be
314 a scrambled, largely undifferentiated jumble of rock and ice. If Mimas turns out to possess
315 these characteristics, then that will provide strong evidence for the scenario outlined here.
316 Conversely, if Mimas turns out to be a differentiated body, then either a heat source
317 post-dating 3.9 Ga capable of causing differentiation but not surface tectonics has to be
318 invoked; or Mimas is younger than 3.9 Ga; or the Nice model explanation for the LHB –
319 when applied to the outer solar system – requires further modification [e.g. *Walsh et al.*,
320 2012].

321 **Acknowledgments.** We thank John Chambers, Fred Ciesla, Sébastien Charnoz, and
322 Alessandro Morbidelli for useful conversations. We also thank both reviewers for their
323 helpful comments. DK was supported by OPR grant NNX11AM57G. NM and EA were
324 supported by PG&G grant NNX13AR66G.

References

325 Asphaug, E. (2010), Similar-sized collisions and the diversity of planets, *Chemie der Erde*
326 - *Geochemistry*, 70(3), 199–219, doi:10.1016/j.chemer.2010.01.004.

- 327 Asphaug, E., and A. Reufer (2013), Late origin of the Saturn system, *Icarus*, *223*(1),
328 544–565, doi:10.1016/j.icarus.2012.12.009.
- 329 Barr, A. C., and R. M. Canup (2010), Origin of the Ganymede–Callisto dichotomy by
330 impacts during the late heavy bombardment, *Nat. Geosci.*, *3*(3), 164–167, doi:10.1038/
331 ngeo746.
- 332 Benz, W., and E. Asphaug (1999), Catastrophic disruptions revisited, *Icarus*, *142*, 5–20.
- 333 Besserer, J., F. Nimmo, J. H. Roberts, and R. T. Pappalardo (2013), Convection-driven
334 compaction as a possible origin of Enceladus’s long wavelength topography, *J. Geophys.*
335 *Res. Planets*, *118*(5), 908–915, doi:10.1002/jgre.20079.
- 336 Canup, R. M. (2010), Origin of Saturn’s rings and inner moons by mass removal from a
337 lost Titan-sized satellite., *Nature*, *468*(7326), 943–6, doi:10.1038/nature09661.
- 338 Charnoz, S., A. Morbidelli, L. Dones, and J. Salmon (2009), Did Saturn’s rings form
339 during the Late Heavy Bombardment?, *Icarus*, *199*(2), 413–428, doi:10.1016/j.icarus.
340 2008.10.019.
- 341 Charnoz, S., A. Crida, J. C. Castillo-Rogez, V. Lainey, L. Dones, O. Karatekin, G. Tobie,
342 S. Mathis, C. Le Poncin-Lafitte, and J. Salmon (2011), Accretion of Saturn’s mid-sized
343 moons during the viscous spreading of young massive rings: Solving the paradox of
344 silicate-poor rings versus silicate-rich moons, *Icarus*, *216*(2), 535–550, doi:10.1016/j.
345 icarus.2011.09.017.
- 346 Chen, E. M. A., and F. Nimmo (2008), Implications from Ithaca Chasma for the
347 thermal and orbital history of Tethys, *Geophys. Res. Lett.*, *35*(19), L19,203, doi:
348 10.1029/2008GL035402.

- 349 Crida, A., and S. Charnoz (2012), Formation of Regular Satellites from Ancient Massive
350 Rings in the Solar System, *Science (80-.)*, 338.
- 351 Dermott, S. F., and P. C. Thomas (1988), The Shape and Internal Structure of Mimas,
352 *Icarus*, 73, 25–65.
- 353 Dermott, S. F., M. Renu, and C. D. Murray (1988), Dynamics of the Uranian and Satur-
354 nian Satellite Systems: A Chaotic Route to Melting Miranda?, *Icarus*, 76, 295–334.
- 355 Dones, L., and H. Levison (2013), The impact rate on Giant Planet satellites during the
356 Late Heavy Bombardment, in *44th Lunar Planet. Sci. Conf. (2013)*.
- 357 Dones, L., C. R. Chapman, W. B. Mckinnon, H. Melosh, M. R. Kirchoff, G. Neukum, and
358 K. J. Zahnle (2009), Icy Satellites of Saturn: Impact Cratering and Age Determination,
359 in *Saturn from Cassini-Huygens*, edited by M. K. Dougherty, L. W. Esposito, and
360 S. M. Krimigis, Johnson 1978, p. 613, Springer Netherlands, Dordrecht, doi:10.1007/
361 978-1-4020-9217-6.
- 362 Gladman, B., and J. Coffey (2009), Mercurian impact ejecta: Meteorites and mantle,
363 *Meteorit. Planet. Sci.*, 44(2), 285–291, doi:10.1111/j.1945-5100.2009.tb00734.x.
- 364 Gomes, R., H. Levison, K. Tsiganis, and A. Morbidelli (2005), Origin of the cataclysmic
365 Late Heavy Bombardment period of the terrestrial planets., *Nature*, 435(7041), 466–9,
366 doi:10.1038/nature03676.
- 367 Kraus, R. G., L. E. Senft, and S. T. Stewart (2011), Impacts onto H2O ice: Scaling laws
368 for melting, vaporization, excavation, and final crater size, *Icarus*, 214(2), 724–738,
369 doi:10.1016/j.icarus.2011.05.016.

- 370 Leinhardt, Z. M., and S. T. Stewart (2012), Collisions Between Gravity-Dominated Bod-
371 ies. I. Outcome Regimes and Scaling Laws, *Astrophys. J.*, *745*(1), 79, doi:10.1088/
372 0004-637X/745/1/79.
- 373 Melosh, H. (1989), *Impact cratering: a geologic process*, 245 pp., Oxford University Press.
- 374 Meyer, J., and J. Wisdom (2007), Tidal heating in Enceladus, *Icarus*, *188*(2), 535–539,
375 doi:10.1016/j.icarus.2007.03.001.
- 376 Monteux, J., G. Tobie, G. Choblet, and M. Le Feuvre (2014), Can large icy moons accrete
377 undifferentiated?, *Icarus*, *237*, 377–387, doi:10.1016/j.icarus.2014.04.041.
- 378 Nagel, K., D. Breuer, and T. Spohn (2004), A model for the interior structure, evolution,
379 and differentiation of Callisto, *Icarus*, *169*(2), 402–412, doi:10.1016/j.icarus.2003.12.
380 019.
- 381 Nesvorný, D. (2011), YOUNG SOLAR SYSTEM’S FIFTH GIANT PLANET?, *Astrophys.*
382 *J.*, *742*(2), L22, doi:10.1088/2041-8205/742/2/L22.
- 383 Nesvorný, D., D. Vokrouhlický, and A. Morbidelli (2013), Capture of Trojans By Jumping
384 Jupiter, *Astrophys. J.*, *768*, 45, doi:10.1088/0004-637X/768/1/45.
- 385 Nimmo, F., and D. Korycansky (2012), Impact-driven ice loss in outer Solar System
386 satellites: Consequences for the Late Heavy Bombardment, *Icarus*, *219*(1), 508–510,
387 doi:10.1016/j.icarus.2012.01.016.
- 388 Owen, J. (2010), ASPH modeling of Material Damage and Failure, in *5th Int. SPHERIC*
389 *SPH Work.*, pp. 297–304, Manchester, United Kingdom.
- 390 Owen, J. (2014), A compatibly differenced total energy conserving form of SPH, *Int. J.*
391 *Numer. Methods Fluids*, *75*, 749–775, doi:10.1002/fld.3912.

- 392 Owen, J., J. Villumsen, P. Shapiro, and H. Martel (1998), Adaptive smoothed particle
393 hydrodynamics : Methodology. II., *Astrophys. J. Suppl. Ser.*, 116, 155–209.
- 394 Sekine, Y., and H. Genda (2012), Giant impacts in the Saturnian system: A possible
395 origin of diversity in the inner mid-sized satellites, *Planet. Space Sci.*, 63-64, 133–138,
396 doi:10.1016/j.pss.2011.05.015.
- 397 Senft, L. E., and S. T. Stewart (2008), Impact crater formation in icy layered terrains on
398 Mars, *Meteorit. Planet. Sci.*, 43(12), 1993–2013, doi:10.1111/j.1945-5100.2008.tb00657.
399 x.
- 400 Shoemaker, E. M., and R. Wolfe (1982), Cratering time scales for the Galilean satellites,
401 in *Satell. Jupiter*, edited by D. Morrison, pp. 277–339, University of Arizona Press.
- 402 Smith, B. A., L. A. Soderblom, R. Batson, F. Bridges, J. Inge, H. Masursky, E. M.
403 Shoemaker, R. Beebe, J. M. Boyce, G. A. Briggs, A. Bunker, S. A. Collins, C. J.
404 Hansen, T. V. Johnson, J. I. M. L. Mitchell, R. J. Terrile, A. F. Cook, J. N. Cuzzi,
405 J. B. Pollack, G. E. Danielson, A. P. Ingersoll, M. E. Davies, G. E. Hunt, D. Morrison,
406 T. Owen, C. Sagan, J. Veverka, R. G. Strom, and V. E. Suomi (1982), A New Look
407 at the Saturn System: The Voyager 2 Images, *Science (80-.)*, 215(4532), 504–537,
408 doi:10.1126/science.215.4532.504.
- 409 Smith, B. A., L. A. Soderblom, R. Beebe, D. Bliss, J. M. Boyce, A. Brahic, G. A. Briggs,
410 R. H. Brown, S. A. Collins, A. F. Cook, S. K. Croft, J. N. Cuzzi, G. E. Danielson,
411 M. E. Davies, T. E. Dowling, D. Godfrey, C. J. Hansen, C. Harris, G. E. Hunt, A. P.
412 Ingersoll, T. V. Johnson, R. G. Kraus, H. Masursky, D. Morrison, T. Owen, J. B. Plescia,
413 J. B. Pollack, C. C. Porco, K. Rages, C. Sagan, E. M. Shoemaker, L. A. Sromovsky,

- 414 C. Stoker, R. G. Strom, V. E. Suomi, S. P. Synnott, R. J. Terrile, P. C. Thomas, W. R.
415 Thompson, and J. Veverka (1986), Voyager 2 in the Uranian System: Imaging Science
416 Results., *Science (80-.)*, *233*(4759), 43–64, doi:10.1126/science.233.4759.43.
- 417 Tajeddine, R., N. Rambaux, V. Lainey, S. Charnoz, A. Richard, A. Rivoldini, and
418 B. Noyelles (2014), Constraints on Mimas’ interior from Cassini ISS libration mea-
419 surements., *Science*, *346*(6207), 322–4, doi:10.1126/science.1255299.
- 420 Thomas, P. C. (1988), Radii , Shapes, and Topography of the Satellites of Uranus from
421 Limb Coordinates, *Icarus*, *73*, 427–441.
- 422 Thomas, P. C. (2010), Sizes, shapes, and derived properties of the saturnian satellites after
423 the Cassini nominal mission, *Icarus*, *208*, 395–401, doi:10.1016/j.icarus.2010.01.025.
- 424 Tsiganis, K., R. Gomes, A. Morbidelli, and H. Levison (2005), Origin of the orbital
425 architecture of the giant planets of the Solar System., *Nature*, *435*(7041), 459–61, doi:
426 10.1038/nature03539.
- 427 Walsh, K. J., A. Morbidelli, S. N. Raymond, D. P. OBrien, and a. M. Mandell (2012),
428 Populating the asteroid belt from two parent source regions due to the migration of
429 giant planets-The Grand Tack, *Meteorit. Planet. Sci.*, *47*(12), 1941–1947, doi:10.1111/
430 j.1945-5100.2012.01418.x.
- 431 Zahnle, K., L. Dones, and H. Levison (1998), Cratering rates on the Galilean satellites.,
432 *Icarus*, *136*(2), 202–22.
- 433 Zahnle, K., P. Schenk, H. Levison, and L. Dones (2003), Cratering rates in the outer Solar
434 System, *Icarus*, *163*(2), 263–289, doi:10.1016/S0019-1035(03)00048-4.

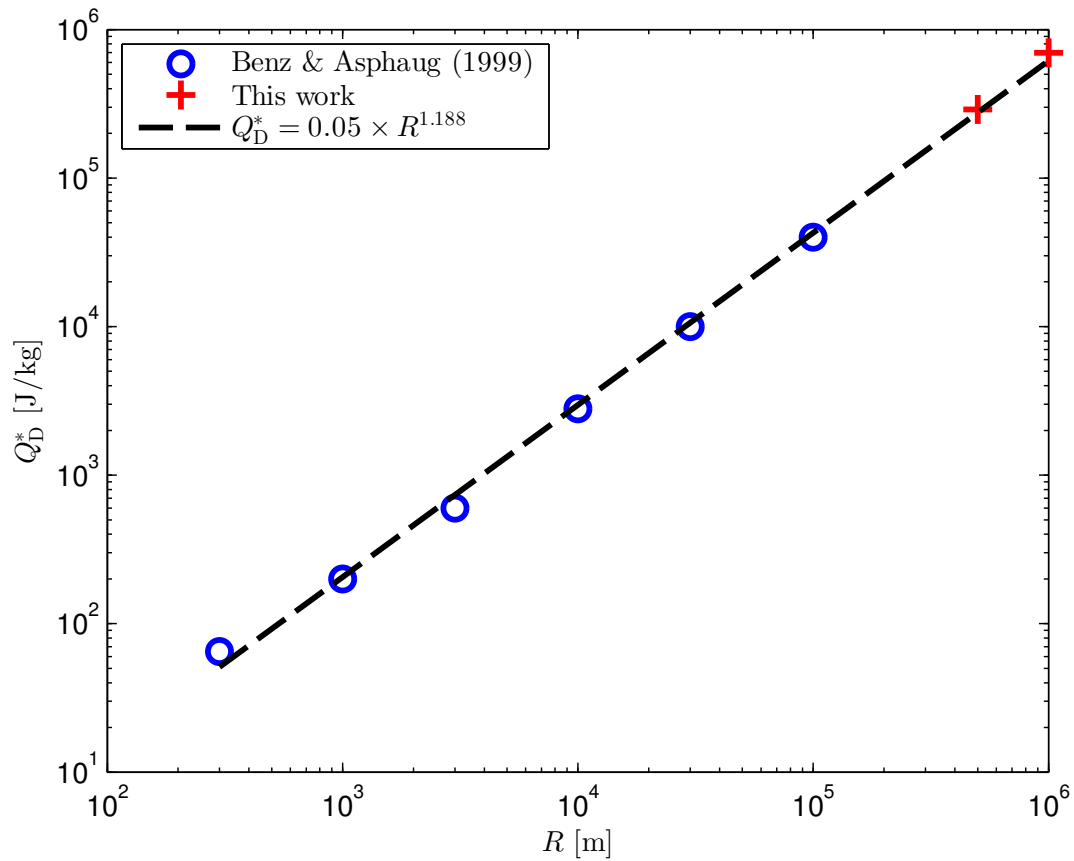


Figure 1. Impact energy required to disperse half the mass (Q_D^*) from an ice target in a gravity-dominated collision as a function of target radius (R) obtained from SPH simulations.

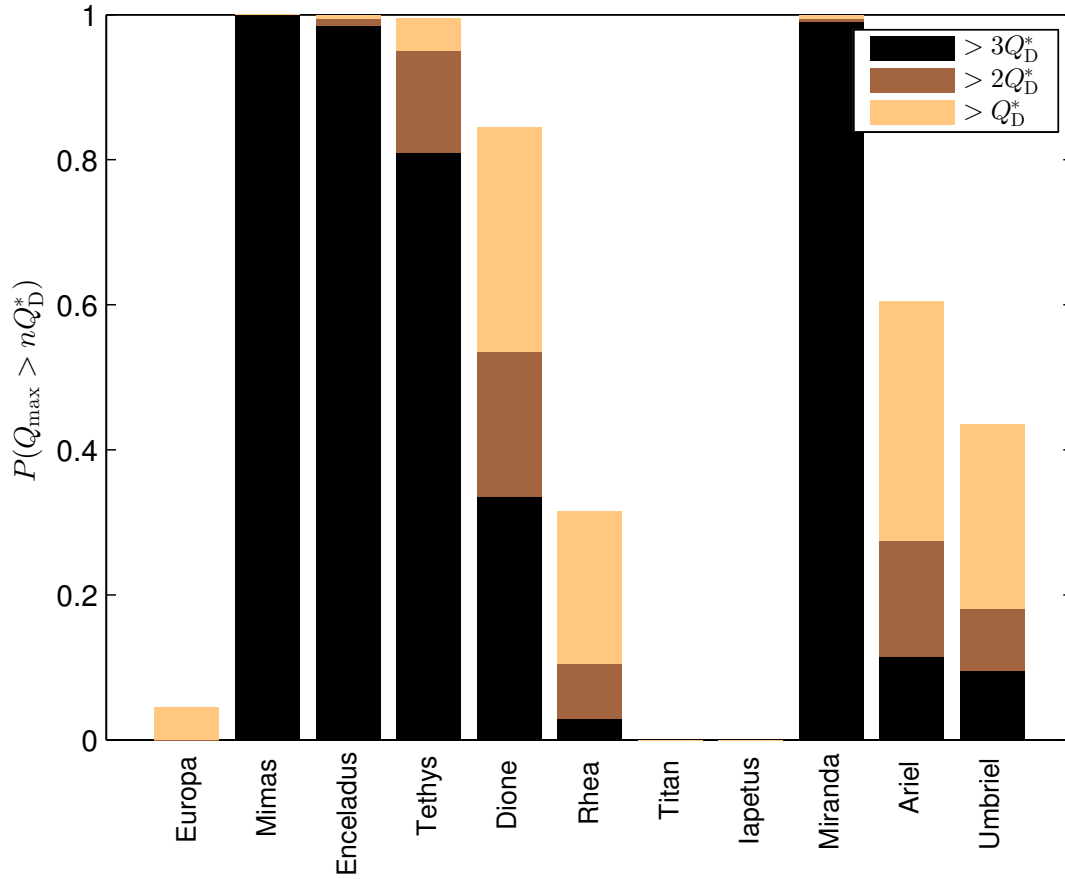


Figure 2. Fraction P of Monte-Carlo runs that included at least one impact with effective specific energy greater than one, two, or three times the catastrophic disruption threshold, Q_D^* . In these runs the mass delivered to each satellite was scaled to deliver $\sim 3 \times 10^{20}$ kg to Callisto [Barr and Canup, 2010].

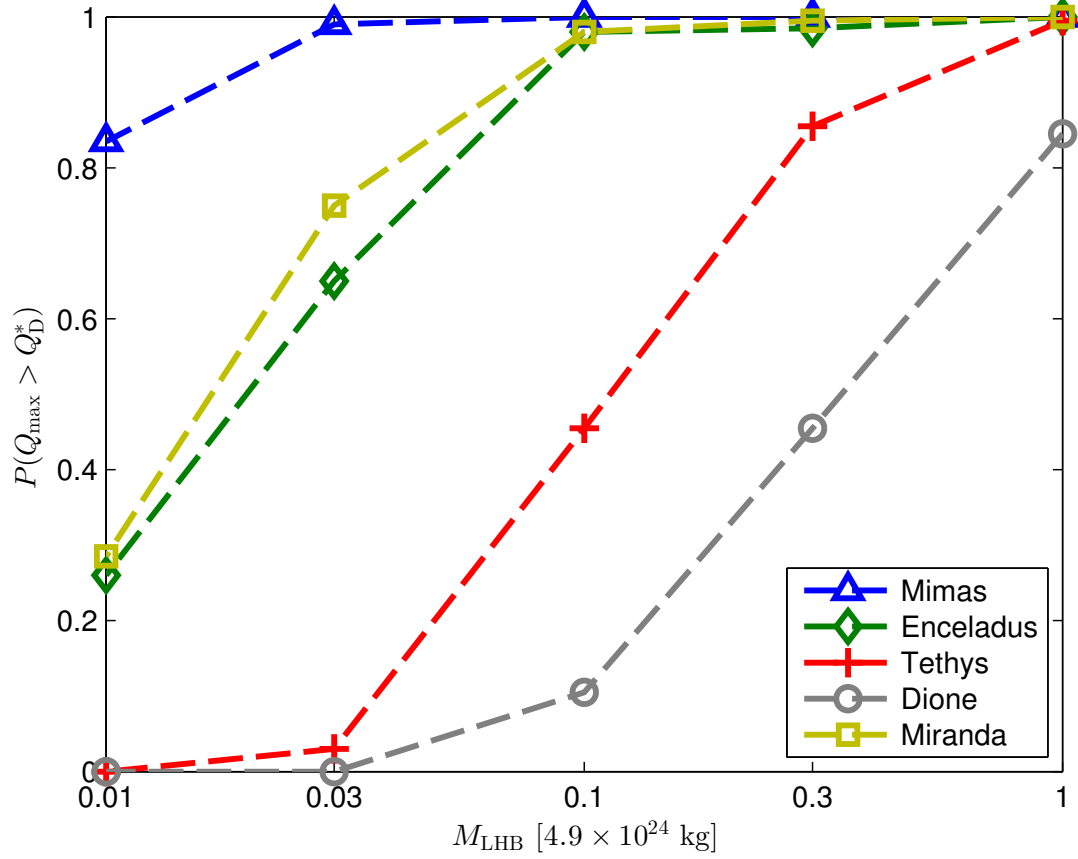


Figure 3. Fraction P of simulations that included at least one catastrophic impact, as a function of total mass delivered. The upper limit value corresponds to 3×10^{20} kg delivered to Callisto.

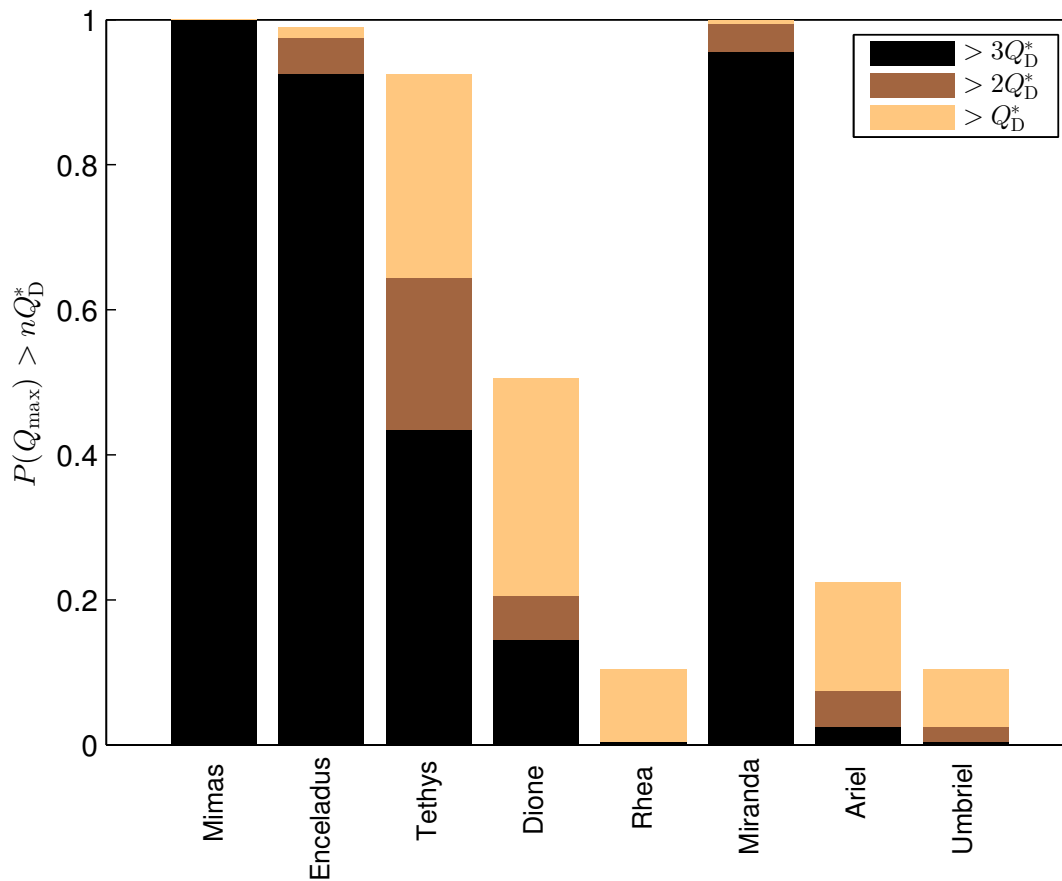


Figure 4. Same as figure 2 but with from runs using a Q_D^* scaling law derived for basalt targets (see text for details).